“Two-steps” process in the first-order transformation of giant magnetocaloric materials

Vincent Hardy, Radia Hamane, Francis Veillon, Michel Risser, François Guillou

“Two-steps” process in the first-order transformation of giant magnetocaloric materials

V. Hardy, R. Hamane, and F. Veillon
Normandie University, ENSICAEN, UNICAEN, CNRS, CRISMAT, 14000 Caen, France

M. Risser
UbiBlue, 23 Boulevard de l'Orangerie, 67000 Strasbourg, France

F. Guillou
Inner Mongolia Key Laboratory for Physics and Chemistry of Functional Materials, College of Physics and Electronic Information, Inner Mongolia Normal University, 81 Zhaowuda Road, Hohhot 010022, Inner Mongolia, People’s Republic of China

ABSTRACT

The most promising materials for applications in magnetic refrigeration exhibit a large entropy change at a first-order ferromagnetic transition. Often, it has been observed that the transformation proceeds via two bursts surrounding a regime of slow transformation. Within a simplified framework, the present article reports on a thermodynamic model able to account for this “two-steps” response. This model is confronted to magnetic and calorimetric data recorded in the magnetocaloric compound $LaFe_{11.4}Si_{1.31}Co_{0.29}$.

Keywords: Phase transformation ; Interfacial misfit ; Gibbs energy; Magnetic properties; La(Fe,Si)$_{13}$ based compound

1. Introduction

Giant magnetocaloric materials have received intense attention over the past two decades, primarily due to their potential applications in magnetic refrigeration that is a technique more environmentally friendly than the conventional gas-vapor technology [1-4]. It turns out that the most promising materials are those exhibiting a large entropy change at a first-order ferromagnetic transition. The dynamics of such a first-order

transition (FOT) involves both a magnetic transformation (between paramagnetic and ferromagnetic states) and a change in the structural parameters (keeping the same symmetry or not, depending on the systems [5]). The dynamical aspect is a crucial issue, not only from a fundamental viewpoint but also for the applicative potential of the magnetocaloric effect [6-10].

Recent studies have revealed peculiar features among which one of the most striking is an exchange of latent heat at the transformation taking the form of a succession of individual peaks as a function of time (yielding "spiky" patterns) [6,11,12]. Another intriguing feature that is often observed is a "two-steps" shape; in this case, the exchange of latent heat mainly exhibits two intense peaks separated by a plateaulike regime [13-15]. In both cases, the basic requirement is a high latent heat confined within a small temperature range, but the conditions for the observation of these particular responses also involve the degree of thermalisation of the sample with the base temperature and the sweep rate of the driving parameter around the transition. While "spiky patterns" require very slow sweep rates and small thermal resistance between the sample and the thermal bath, less stringent conditions seem to be necessary for the observation of the "two-steps" shape.

Various manifestations of the "two-steps" response can be found in the literature; it turns out that the greatest part of these studies were carried out in the $La(Fe,Si,Mn,Co)_{13}$ system which is the most investigated magnetocaloric family nowadays. In one of the first investigations of the transitional kinetics in these materials, Fujita et *al.* reported a clear two-steps signature in the cooling curve of $LaFe_{11.44}Si_{1.56}$ [13]. Two-steps patterns were also observed in the percentage of transformation between the two phases around the T_C, derived either from x-ray diffraction in $LaFe_{11.8}Si_{1.2}$ [16] or from magnetization measurements in $LaFe_{11.7}Co_{0.195}Si_{1.105}$ [17]. Moreover, one can note that the profiles of

heat flux exchanges detected by differential scanning calorimetry (DSC) based on Peltier cells ($LaFe_{11.41}Mn_{0.30}Si_{1.29} - H_{1.62}$ in [14]) or from the thermopile voltage in a microcalorimeter ($LaFe_{11.74}Mn_{0.06}Si_{1.20}$ in [8]) exhibited a shape dominated by two well-separated large peaks.

The goal of the present paper is to suggest a qualitative explanation for this type of two-steps process, on the basis of a simple thermodynamic approach.

2. Experimental details

The study was carried out on an industrial material belonging to the $La(Fe,Si,Co)_{13}$ family provided by Vacuumschmelze GmbH and CoKG. Compositional analyses carried out by energy-dispersive x-ray spectroscopy in a scanning electron microscope (Hitachi SU8010 equipped with IXRF systems spectrometer) lead to the formula $LaFe_{11.4}Si_{1.31}Co_{0.29}$. Different samples from the same batch and with the same size ($2.2\times2.2\times0.4$ mm^3) were used for magnetic and calorimetric measurements.

Magnetization curves as a function of temperature, *M(T)*, were recorded in a commercial device (PPMS, Quantum Design), at a slow sweep rate crossing the transition both upon warming and cooling, in a small magnetic field of 100 Oe. Two types of calorimetric measurements were recorded in zero-field. Firstly, specific heat curves, *C(T)*, were derived from an home-made Peltier-based calorimeter, employing a Quantum Design Versalab system for temperature control, a Keithley 2182A nanovoltmeter for recording the potential difference and RMT (model 1MD03- 018) miniature thermoelectric elements mounted in differential configuration as sensors. Secondly, relaxation curves were recorded in the semi-adiabatic configuration of the specific-heat option of the PPMS: the sample is pasted on a sapphire platform at the bottom of which are placed a heater and a thermometer; this platform is connected to the system by wires

which ensure the thermal contact with the base temperature; after stabilization at the base temperature ($T < T_C$), heating power triggers an increment of temperature (up to $T > T_C$), then it is shut down. In the present work, we focus on the last stage of the process, i.e. the relaxation curve along which the temperature of the sample decreases with time down to the base temperature while crossing T_C.

3. Results

3.1. Experimental data

Figure 1(a) shows *M(T)* curves recorded around the transition, at a rate of 0.1 K/min. One clearly observes hysteresis and a transition that proceeds by steps. The density of data points is limited by the combination of the sweep rate and of the intrinsic duration of each measurement (~ 15 s) leading to a spacing of ~ 0.03 K. It is on the cooling curve that the "two-steps" shape is the most visible, a feature already noted in previous studies [16-17].

Figure 1(b) shows specific-heat data measured in the DSC device when using the same rate of 0.1 K/min. On each branch (either cooling or warming), one observes a steep rise at the beginning of the transition, followed by a slowdown and finally a large peak at the end; this sequence yields an overall shape that can be regarded as double peak. Let us specify that the discrepancies in the values of the transition temperature between Figs 1(a) and 1(b) can be mainly ascribed to a variation in the thermometry of the devices (dealing primarily with the calibration of the thermometers and the degree of thermalisation of the samples).

Figure 1(c) displays the relaxation curve *T(t)* from 211 K ($T > T_C$) to the base temperature 206 K ($T < T_C$) recorded using the semi-abiabatic calorimetric option. A plateau marking the development of the FOT is clearly visible. The enlargement displayed

in Fig. 1(d) shows that this transitional regime is made of a plateau surrounded by two sharp increases in temperature (marked by arrows).

Panels (e) and (f) illustrate the reproducibility of the phenomenon. Qualitatively, the same two-steps feature is observed in various samples for given procedure (e.g. a fixed cooling rate), as well as for different procedures when using the same sample (with the same mounting).

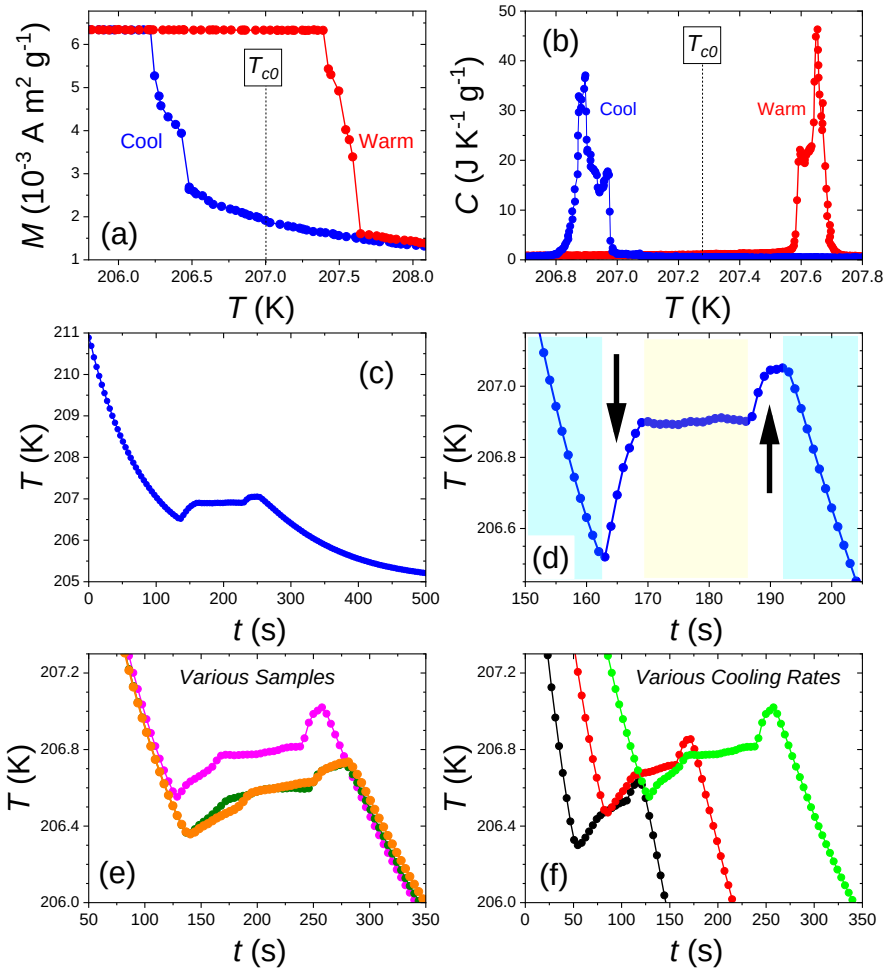

Fig.1 : Physical properties of $LaFe_{11.4}Si_{1.31}Co_{0.29}$. (a) Magnetization recorded in 100 Oe at 0.1K/min; (b) Specific heat recorded by DSC in zero-field at 0.1 K/min; (c) Relaxation curve across the T_C in zero-field; (d) Enlargement of (c) around the transition. The cyan areas mark the regimes out of the transition, the white areas correspond to the bursts, and the yellow area is the intermediate regime with very slow transformation; (e) Comparison of the relaxation curves of different samples measured with the same procedure or (f) of different procedures applied to the same sample.

It deserves to be noted that the two types of calorimetric data are consistent with each other if one admits that the peaks in Fig. 1(b) correspond to bursts in the release of latent heat yielding the rises of temperature on each side of the plateau in Fig. 1(d). Furthermore, we emphasize that the thermal data are well complemented by the magnetic ones. Indeed, the magnetization does not probe the exchange of heat, but it directly reflects the degree of phase transformation, a piece of information which is lacking in calorimetric experiments. Combining these techniques suggest that sudden advances in the phase transformation are concomitant with sudden changes in exchange of heat. The largest events take place at the beginning and end of the transformation, constituting what is referred to as the “two-steps” response in this article.

3.2. Model

The starting idea was to explore the possibility of a transformation path energetically more favorable than a continuous switching between the two phases. We do not pretend to go beyond a "toy model", because we will neglect the details of the microstructure, while it is known to be a key aspect for the development of the FOT in this type of materials [18]. Our approach involves the observation that the transformation generally starts from the edges of the sample, and then progressively invades it till its center [19]. This feature is particularly marked for the PM-to-FM transformation, as attested to by magneto-optics experiments [6,17]. In what follows, one considers this PM-to-FM direction of the transition (which is that of the relaxation curves). It can be noted that the development of the ferromagnetism from the sides is qualitatively consistent with the fact that the external surfaces can help to accommodate the greater unit-cell volume of the FM phase. Another important issue to be taken into account is that the problem requires to consider the sample as a whole, with its own volume and surface. For the sake

of generality and simplicity, we will assume a cubic sample of side L_0. One also assumes an isotropic progress of the transition that can be tracked by a single parameter L corresponding to the side of the internal cube of material that is not yet transformed.

Within the frame of these approximations, the simple picture of the transition considered in this paper is shown in Fig. 2. We are examining the possibility of two bursts along the transformation, the first one at L_1 and the second one at L_2; in between ($L_2 < L < L_1$) the transformation can be gradual. The driving parameter of the transition is the temperature (at least till reaching T_C), but along the transformation itself, it can also be the time per se. The compounds of the La(Fe,Si,Mn,Co)$_{13}$ system exhibit a cubic-to-cubic structural change at the T_C [20-21] As schematically displayed in Fig. 2(f), the unit-cell volume V is larger in the FM state, with a relative change (dV/V) of the order of 1%; thereafter, one considers the relative increase in the unit-cell parameter i.e., $p = \frac{1}{3}\frac{\Delta V}{V}$. Owing to the negative step in $V(T \sim T_C)$, the application of pressure shifts the transition towards lower temperature.

Along the PM-to-FM transformation, one expects the development of strain at the boundary and of long-range stress from these boundaries [22]. This stress induces an increase in pressure in the central part of the sample that is not yet transformed. Figures 2(g-i) illustrate schematically the way one takes into account the change of pressure associated with the progression of the transformation. In the range $L_2 < L < L_1$, the variation from L to $L+dL$ ($dL < 0$) is decomposed into two parts: first, a *virtual* transformation PM-to-FM of a slab δL without change of unit -cell; then, the application of the strain $\varepsilon \sim p$ to reach the increment $dL = \delta L(1+p)$. It is this latter part which induces an increase of (internal) pressure at long range. This is a crucial issue since the T_C (thereby, the strength of the driving force of the transformation at a given temperature T) depends on the pressure.

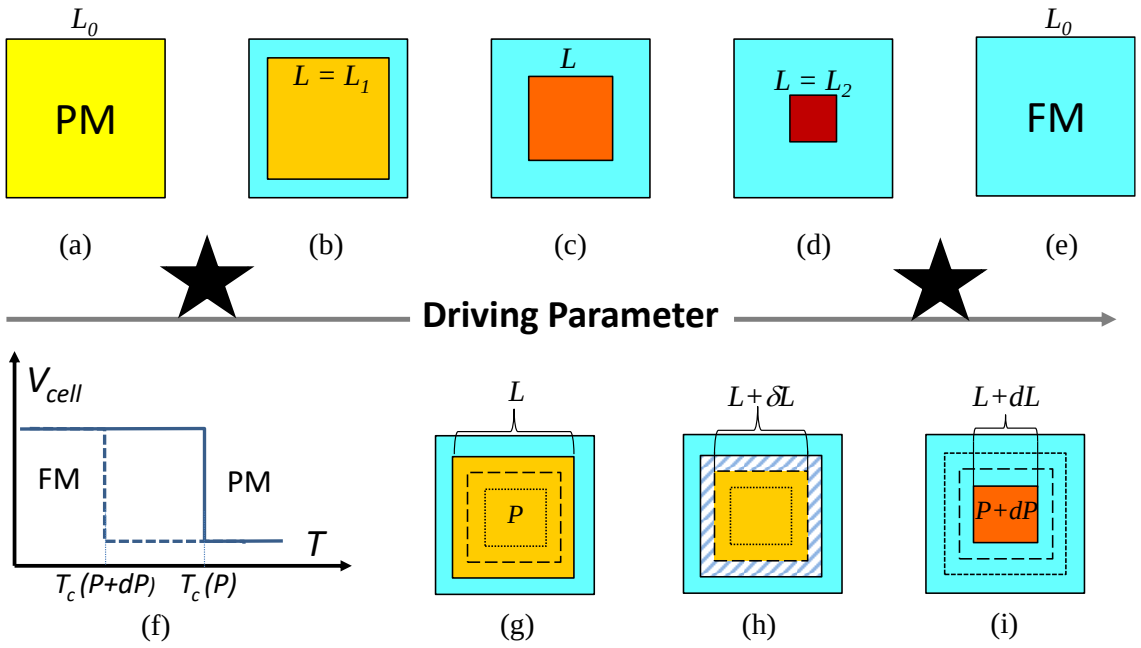

Fig. 2 : The top panels are pictures of the suggested stages of the PM-to-FM transformation: (a) pure PM state; (b) mixed state after the first burst; (c) mixed state in the intermediate regime; (d) mixed state just before the second burst; (e) full FM state reached after this second burst. Blue is for the FM phase, while the color for PM evolves from yellow (stress-free) to red as the pressure is increased. The stars show the location of the bursts along this evolution. The bottom panels focus on the pressure effect: (f) shows the impact on the T_C, while the set (g-i) illustrates the approach used to estimate the relationship between L and the internal pressure P (see text).

Figure 3(a) schematically illustrates this relationship by showing the Gibbs free energy lines, $G(T)$, of the PM and FM states for zero ($L = 0$ or $L = L_0$) and non-zero pressure ($0 < L < L_0$). For simplicity, the pressure effect in this plot is entirely ascribed to the PM state, that is acceptable since the important parameter in the end is the driving force, i.e. the *difference* between the two states. Note also that we approximate the real temperature dependencies by linear curves, which is another reasonable simplification if we limit ourselves to the region around the transition. These lines refer to each state individually, without interaction between them. In principle, the transition from one state to the other is expected to take place at the crossing point between these lines [see Fig. 3(a)]. In practice, however, extra energy terms come into play when considering how the

transformation can proceed. It turns out that these terms tend to hinder the transition, in such a way that a larger shift ΔG is necessary to trigger the transformation; consequently, the transformation actually starts at a temperature T_{tr} lower than the underlying T_C. The shift between the Gibbs energy of each pure state is often referred to as the chemical driving force, ΔG. For practical reasons, we consider $\Delta G = G_{PM} - G_{FM}$, which means that the transition PM to FM corresponds to positive ΔG.

It turns out that a relationship can be established between $\Delta G(T)$ and the entropy jump at the transition, noted ΔS_{tr} [see Fig. 3(b)]. Figure 3(a) allows us to approximate (a, b, c, and d being numerical constants) $G_{PM}(T) = a + b \times T$ and $G_{FM}(T) = c + d \times T$. At T_C, one has by definition $G_{PM}(T_C) = G_{PM}(T_C)$, thus $a + b \times T_C = c + d \times T_C$. Introducing the thermodynamical relationship $S = -\frac{dG}{dT}$, where S is the entropy, one derives: $a - c = (d - b)T_C = [-S_{FM}(T \lesssim T_C) + S_{PM}(T \gtrsim T_C)]T_C = \Delta S_{tr} \times T_C$. Therefore, one obtains

$$\Delta G(T) = G_{PM}(T) - G_{FM}(T) = (a - c) + (b - d)T = \Delta S_{tr}(T_C - T) \qquad (1)$$

We emphasize that the transformation is considered to develop at a temperature $T = T_{tr}$ that is slightly lower than the T_C (as defined above).

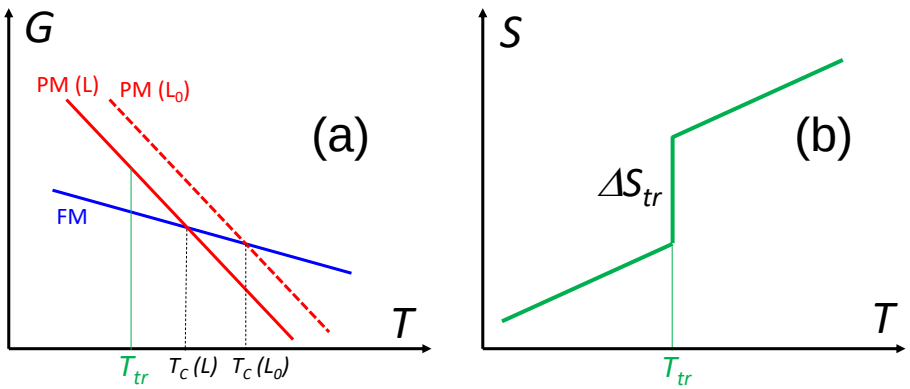

Fig. 3 (a) Schematic picture of the Gibbs free energies of the FM and PM states. For the latter, two curves are drawn corresponding to zero or non-zero internal pressure. The crossings between the FM and PM curves define the underlying T_C values. However, owing to other energy terms (see text), the driving force

has to reach a certain value to trigger the transformation at a temperature T_{tr} lower than T_C. Panel (b) is a schematic picture of the entropy jump at T_{tr}.

In Fig. 2, the top row of panels is a schematic picture of the suggested transformation path to account for the existence of the two bursts. The degree of progress of the transition is followed by the variable L that must go from L_0 to 0. Panel (a) is the starting point, corresponding to a purely PM state. We consider that the system is at a temperature $T \lesssim T_C(L_0) = T_{C0}$, for which the transformation PM-to-FM should have started without the presence of energy terms related to the mechanical friction between the two phases [Fig 3(a)]. Actually, the increase in energy associated with the structural mismatch at the interface is such that the transition cannot start yet. Between (a) and (b), there is an undercooling regime along which the driving force $\Delta G(T, L_0)$ increases, but the transition remains blocked. Panel (b) shows the stage where $\Delta G(T, L_0)$ exceeds the threshold required to trigger the first burst: the FM phase suddenly enters the sample till reaching $L = L_1$. Panel (c) illustrates a regime of progressive development of the transformation that is controlled by the stress-induced decrease of $\Delta G(T, L)$. Panel (d) corresponds to the stage where it becomes beneficial for the system to eliminate the interfacial energy (PM/FM) by switching abruptly to the fully FM state. This process is ascribed to the second burst, leading to a purely ferromagnetic state that is displayed in panel (e). This transformation path thus goes through two bursts (marked by the two black stars in Fig. 2). In practice, the release of latent heat at each of these bursts is expected to be so sudden that a transitory increase in the sample temperature can hardly be avoided.

Let us now explore the possibility to account for such a path within a thermodynamical approach. We use hereafter lower case letters (g) for the total enthalpy of the sample, including all relevant terms, while upper case letters (G) correspond to the (intrinsic) volume enthalpies of the FM or PM states. There are three expressions of the

Gibbs free energy of the sample to be compared: (i) g_{PM} for the "full PM" state ($L = L_0$), as shown in Fig. 2(a); (ii) g_{FM} for the « full FM » state ($L = 0$) of Fig. 2(e); and (iii) g_{mix} for a "mixed" state ($L_0 < L < 0$), combining PM and FM parts, as illustrated in Fig. 2(c). For the first two cases, the sample Gibbs free energy can be simply written as (the variable L_0 meaning the absence of internal pressure):

$$g_{PM}(T) = L_0^3\, G_{PM}(T, L_0) \qquad (2a)$$

$$g_{FM}(T) = L_0^3\, G_{FM}(T, L_0) \qquad (2b)$$

The case of g_{mix} is more complex, since it is a combination of several terms. Adopting the terminology used for the martensitic transformations, we will consider g_{chem} , g_{inter} and g_{elas}, being the chemical, interfacial, and elastic terms, respectively [23-24]. The g_{chem} term depends on the volumic fractions of each of the two states; in the mixed regime, a volume (L_0^3-L^3) has become FM, leading to $g_{chem}(T, L) = (L_0^3 - L^3)G_{FM}(T) + L^3 G_{PM}(T, L)$. In connection with Fig. 3(a), we include explicitly the variable L in G_{PM} to indicate that the internal pressure is taken into account. By introducing the pressure- and temperature-dependent "chemical driving force" $\Delta G(T, L) = G_{PM}(T, L) - G_{FM}(T)$, one can write

$$g_{chem}(T, L) = L_0^3 G_{FM}(T) + L^3 \Delta G(T, L) \qquad (3)$$

The coexistence of PM and FM domains yields stress between them owing to the difference in unit-cell volumes. First, this generates an increase of energy associated to the boundaries between the two phases, corresponding to g_{inter}. Second, the displacement of this boundary induces a structural distortion and thus an elastic energy corresponding to g_{elas}. Lastly, one should also consider the pressure effect at longer range, but this is already taken into account via the L dependence of $\Delta G(T, L)$ in g_{chem}.

Let us consider the surface energy λ of the interface PM/FM, which reflects the friction between the two phases at the front separating them. In the simple picture of Fig. 2, there is a contact area of $6L^2$ as soon as $L \neq L_0$, leading to

$$g_{inter}(T,L) = 6\lambda L^2 \qquad (4)$$

Note that this interfacial energy must be distinguished from the surface tension that is involved in calculations of critical sizes for nucleation [23].

The elastic term derives from the combination of the stress (σ) and strain (ε) within the transformed zone. Per unit volume, one expects a contribution of the type, $\sigma\varepsilon = \frac{B}{1-\nu}\varepsilon^2$, where B is the average bulk modulus of the two phases around T_C, ν the Poisson's ratio and $\varepsilon \sim p$. Each variation by dL (< 0) corresponds to a volume $-3L^2dL$, thus the integration along the transformation (from L_0 to L) yields

$$g_{elas}(T,L) = \int_{L_0}^{L} \frac{Bp^2}{1-\nu}(-3L^2dL) = \frac{Bp^2}{1-\nu}(L_0^3 - L^3) \qquad (5)$$

Adding these various terms ($g_m = g_{chem} + g_{inter} + g_{elas}$), one arrives at

$$g_m(T,L) = L_0^3\left\{G_{FM}(T) + \left(\frac{Bp^2}{1-\nu}\right)\right\} + L^3\left\{\Delta G(T,L) - \left(\frac{Bp^2}{1-\nu}\right)\right\} + 6\lambda L^2 \qquad (6)$$

The problem at this stage is to evaluate the dependence of ΔG on L. One can start from

$$\Delta G(T,L) = \Delta G(T,L_0) + \int_{L_0}^{L} \frac{d\Delta G(T,L)}{dL}dL = \Delta S_{tr}(T_{C0} - T) + \int_{L_0}^{L} \frac{d\Delta G(T,L)}{dL}dL \qquad (7)$$

Let us now use the composition

$$\frac{d\Delta G(T,L)}{dL} = \frac{d\Delta G(T,L)}{dT_C} \times \frac{dT_C}{dP} \times \frac{dP}{dL} \qquad (8)$$

In practice, $\frac{dT_C}{dP}$ is a parameter which can be extracted from the literature, while Eq. (1) shows that $\frac{d\Delta G(T)}{dT_C} = \Delta S_{tr}$. As for $\frac{dP}{dL}$, it can be related to the bulk modulus B as shown in Fig. 2 (g-i). Indeed, the increase of pressure dP resulting from the volume expansion within the transformed region [from δL to $dL = \delta L(1+p)$] can be evaluated by $dP =$

$-B\frac{3(L+\delta L)^2 p\delta L}{(L+\delta L)^3} = \frac{-3Bp\frac{dL}{1+p}}{L\left(1+\frac{\delta L}{L}\right)}$. Considering that $p << 1$ and $\delta L/L << 1$, this relationship can be approximated by $\frac{dP}{dL} \sim \frac{-3Bp}{L}$. Re-injecting these expressions into Eq. (8), one arrives at

$\frac{d\Delta G(T,L)}{dL} = \Delta S_{tr} \times \left(\frac{dT_C}{dP}\right) \times (\frac{-3Bp}{L})$, and from Eq. (7) one obtains

$$\Delta G(T,L) = \Delta S_{tr}(T_{C0} - T) + \Delta S_{tr} \times \left(\frac{dT_C}{dP}\right) \times (-3Bp) \times \ln(\frac{L}{L_0}). \quad (9)$$

Turning back to g_m [Eq. (6)], this yields

$$g_m(T,L) = L_0^3 \left\{ G_{FM}(T) + \left(\frac{Bp^2}{1-\nu}\right)\right\} + L^3[\Delta S_{tr}(T_{C0} - T) +$$

$$\Delta S_{tr} \times \left(\frac{dT_C}{dP}\right) \times (-3Bp) \times \ln(\frac{L}{L_0}) - \left(\frac{Bp^2}{1-\nu}\right)] + 6\lambda L^2 \quad (10)$$

Let us introduce two positive constants :

$$X = \Delta S_{tr} \times \left(\frac{dT_C}{dP}\right) \times (-3Bp) \quad (11a)$$

$$Y = \left(\frac{Bp^2}{1-\nu}\right) \quad (11b)$$

The three expressions of the sample Gibbs free energy to be considered become:

$$g_{PM}(T) = L_0^3\, G_{PM}(T, L_0) \quad (12a)$$

$$g_m(T,L) = L_0^3[G_{FM}(T) + Y] + L^3[\Delta S_{tr}(T_{C0} - T) - Y] + L^3\, X \ln\left(\frac{L}{L_0}\right) + 6\lambda L^2 \quad (12b)$$

$$g_{FM}(T) = L_0^3\, G_{FM}(T, L_0) \quad (12c)$$

Since the point is a *comparison* between these terms, one can consider relative quantities. Relative energies denoted by g^* are obtained by (i) dividing the above expressions by L_0, (ii) subtracting $G_{FM}(T, L_0)$, and (iii) introducing the parameter $z = L/L_0$. Doing so, one obtains

$$g^*_{PM}(T) = \Delta S_{tr}(T_{C0} - T) \quad (13a)$$

$$g^*_{mix}(T,L) = Y + z^3[\Delta S_{tr}(T_{C0} - T) - Y] + z^3\, X \ln z + 6\left(\frac{\lambda}{L_0}\right) z^2 \quad (13b)$$

$g^*_{FM}(T) = 0$ (13c)

The most stable state at a temperature *T* is expected to be the one yielding the lowest *g*(T)* value.

4. Discussion

At this stage, one must evaluate the model parameters. For most of them, reasonable estimates can be extracted from the literature.

-*Bulk modulus*. In a Co-free compound, $LaFe_{11.18}Si_{1.82}$, (with $T_C \sim 210$ K), high-pressure x-ray diffraction experiments yield a bulk modulus $B \sim 125$ GPa [25]. In a composition closer to ours, ($LaFe_{11.74}Co_{0.13}Si_{1.13}$), the same approach led to $B \sim 100$ GPa [9]. The same order of magnitude (80-110 GPa) was also obtained from mechanical techniques in $LaFe_{11.09}Co_{0.86}Si_{1.05}$, $LaFe_{10.81}Co_{1.18}Si_{1.01}$, $LaFe_{10.63}Co_{1.33}Si_{1.04}$, and $LaFe_{10.54}Co_{1.43}Si_{1.03}$ [26].

-*Poisson's ratio.* For the type of alloys one deals with, it is customary to consider the approximation $\nu \sim 0.3$ [19,27,28]

-*Pressure dependence of* T_C. Actually, there are not so many data about this pressure dependence. In the case of $LaFe_{11.44}Si_{1.56}$ and $LaFe_{11.18}Si_{1.86}$, Fujita *et al.* reported $\frac{dT_C}{dP} \sim -93$ and -68 K(GPa)$^{-1}$, respectively [20]. Studying the impact of hydrogenation, Lyubina *et al.* found $\frac{dT_C}{dP} \sim -222$ and -99 K(GPa)$^{-1}$ in $LaFe_{11.57}Si_{1.43}$ and $LaFe_{11.57}Si_{1.43}$-$H_{1.64}$, respectively [29]. Recently, Hao *et al.* reported in a Co-containing material, $LaFe_{10.95}Co_{0.95}Si_{1.1}$, the value $\frac{dT_C}{dP} \sim -83$ K(GPa)$^{-1}$ [30].

-*Isomorphic change*

In the La(Fe,Si,Co)$_{13}$ family, $\Delta V/V$ is of the order of 1%, [20-21] thus $p \sim 0.01/3$.

-*Entropy jump*. Using the Clausius-Clapeyron equation applied to magnetic data in samples of the same batch, the entropy change at T_C in low field is estimated to ~13 $JK^{-1}kg^{-1}$ [31]. With a density of ~7.2 g/cm^3, it yields $\Delta S_{tr} \sim 9.4\ 10^4\ JK^{-1}m^{-3}$.

-*Undercooling.* According to the curves of Fig. 1, (T_{c0} -T) is estimated to be within the range 0.3-1 K.

-*Sample size.* Even though our samples have a parallepipedic shape (2.2×2.2×0.4 mm^3), whereas the model assumed a cubic one, one can consider that the characteristic length L_0 is of the order of one millimeter [$(2.2\times2.2\times0.4)^{1/3}$ =1.24)].

-*Interfacial energy.* Actually, this parameter is the least well-known. According to [23], the interfacial energy solid-solid in metallic materials is thought to be of the order of 0.5 J m^{-2}. However, this corresponds to a local value, whereas the λ introduced in Eq. (4) is a macroscopic quantity; it is actually a phenomenological value which should incorporate the fact that the actual contact area at the microscopic scale is obviously much larger than the oversimplified geometrical surface assumed in the model (Fig. 2).

We took the option to let free only this λ parameter, while fixing typical values for all the other parameters for which reasonable approximations were available. We assumed the following values : B = 100 GPa ; ν = 0.3 ; $\frac{dT_C}{dP} = -100\ K(GPa)^{-1}$; p = 0.003 ; $\Delta S_{tr} = 10^5\ JK^{-1}m^{-3}$; (T_{c0}-T) = 0.5 K ; $L_0 = 10^{-3}$ m. To reproduce the experimental behavior [Fig. (1)], the mixed state needs to be the most favorable within the intermediate z range. With the assumed set of parameters, we found that this requires λ to be of the order of 50 J m^{-2}.

The relative Gibbs free energies of the pure PM, the pure FM and the mixed states are plotted in Fig. 4 for the displayed set of parameters. It shows a crossing between PM and mixed states at L_1/L_0 = 0.936, and another one between mixed and FM states at L_2/L_0 = 0.654. This means there are two ranges of z values that are *energetically unfavorable*

for a mixed state : $L_1 < L < 1$ and $0 < L < L_2$. This is qualitatively consistent with the observations. Inset (b) shows the same data but with circles marking the expected magnetic states: by definition, full PM and full FM correspond to $z = 1$ and $z = 0$, respectively; for the mixed state, one can either envision a continuous evolution of states within the range L_1-L_2 (open circles) or consider that the system will lock itself to the state of minimal g_m at $z \sim 0.8$ (full green circle).

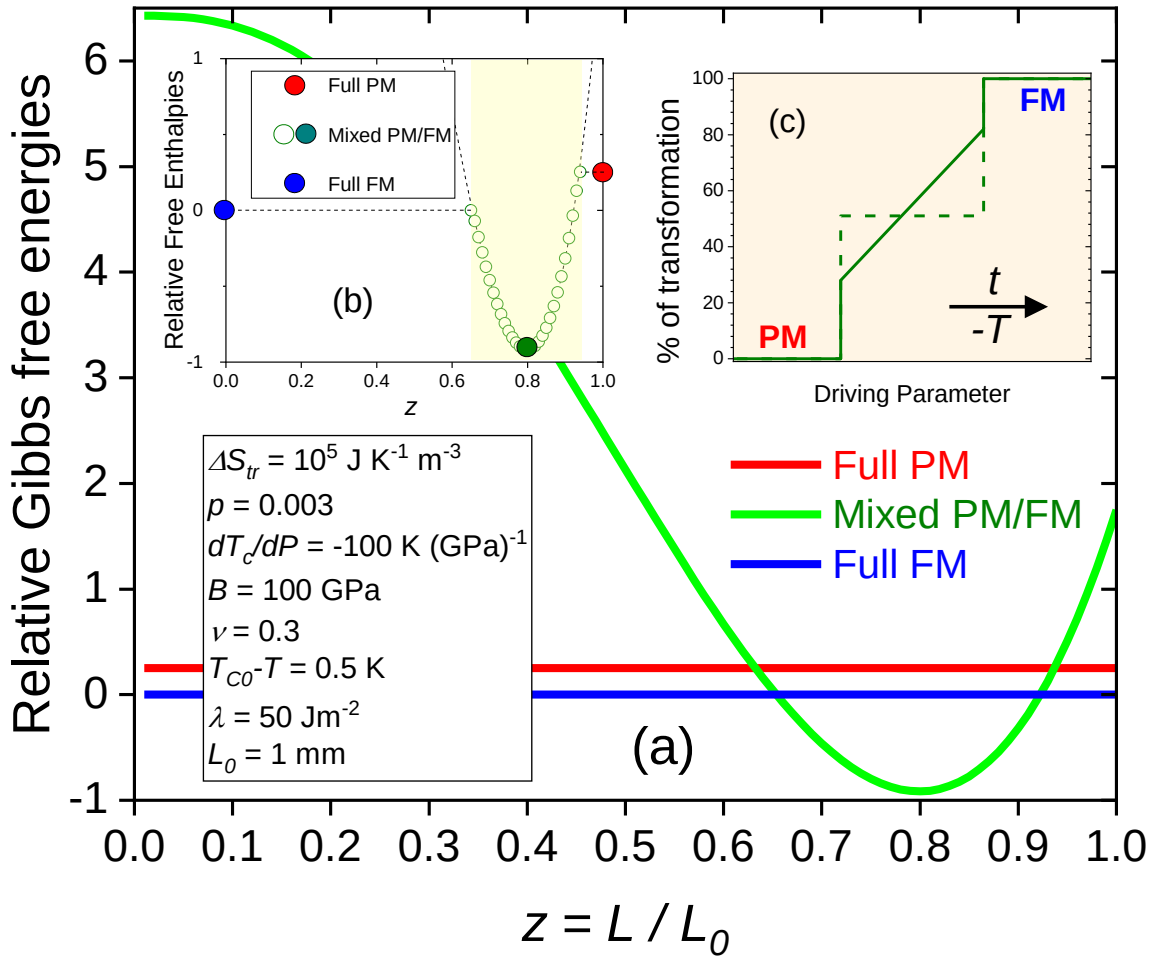

Fig. 4: Main panel (a) shows the relative Gibbs free energies as a function of the penetration depth of the transformation (see Fig. 2) for the three states: full PM, full FM and mixed state calculated from Eqs (13) with the values of parameters displayed in the legend. Inset (b) converts this data in terms of states (circles): the full PM and full FM corrrespond to z =1 and z = 0, respectively; the mixed state can take place over the z range highlighted in yellow (yielding states corresponding to open circles), but the most stable state minimizing the energy is that marked by the filled circle. Inset (c) converts inset (b) in percentage of phase transformation as a function of the driving parameter, considering for the mixed state either the most stable state only (dashed line) or all the available z-range (full line).

These evolutions are represented in inset (c) in terms of percentage of transformation ($\propto z^3$) as a function of the driving parameter (i.e., decreasing temperature or increasing time when the transformation is taking place). One observes two jump-like evolutions at the beginning and end of the transition and a more progressive transformation in between, which is in remarkable qualitative agreement with the data presented in Fig. 1. Our results are also consistent with several studies of the literature such as magnetic data in $LaFe_{11.7}Co_{0.195}Si_{1.105}$ [17] and the fraction of transformed phase derived from x-ray diffraction in $LaFe_{11.8}Si_{1.2}$ [16]. In this latter study, Waske et *al.* have proposed an interpretation of this peculiar shape of transition within the assumption of a sample regarded as an "agglomerate of particles". The first step is ascribed to a stage of easy phase transformation, facilitated by the interspacing between particles which allows to accommodate the volume changes; then, the plateau corresponds to a blocking of the transformation occurring when these internal spaces have disappeared, and finally, the last step is qualitatively attributed to a brutal jump occurring when the driving force overwhelms the energy barrier.

In this vision and ours, the basic ingredient is the change of intrinsic volume which accompanies the transformation, but the interpretations differ. In [16] a basic role is ascribed to a specific microstructure made of rather loose individual particles. Our picture is the opposite extreme since the sample is regarded as a "monolithic" piece, neglecting all the details of the microstructure. Clearly, the two visions are oversimplified with respect to the actual complexity of the microstructure [32]. A numerical approach could help to be more realistic by introducing some important features of the microstructure such as secondary phases, grain boundaries, cracks, voids and so on.

5. Conclusion

The “two-steps” process encountered in some first-order transitions refers to the fact that the transformation starts and ends by sudden changes in the transformed fraction that are accompanied by large exchanges of latent heat (leading to transitory changes in temperature since the thermalisation cannot immediately absorb such bursts of heat). In the present work, we propose a simple thermodynamic model which can account for this behavior by considering a Gibbs free energy of the mixed state including three terms: chemical, elastic and interfacial. The pressure stemming from long-range stress is incorporated into the chemical term. Comparison of the Gibbs free energies of mixed state with fully PM or fully FM states can explain a first jump from PM to a mixed PM/FM state, then a regime of mixed state where the transformation is blocked or at least very slow, and a final jump to pure FM.

The first step bears similarity with usual recalescence at the beginning of a transformation after undercooling. However, it is not a matter of critical volume as in homogeneous nucleation, but it rather results from the fact that the start of the transition has a high price to pay in terms of interfacial energy (since developping from the external surfaces). The second step is more unusual. In our model, it corresponds to the fact that it becomes prohibitively expensive in energy for the system to keep a small fraction of untransformed material (since combining high internal pressure and large surface/volume ratio). To go further, simulations should be carried out to allow taking into account some important aspects of the microstructure and to consider a more realistic shape for the transformation front.

Declaration of Competing Interest

The authors declare that they have no known competing financial interests or personal relationships that could have appeared to influence the work reported in this paper.

Acknowledgments

This work was supported by the project CoolMagEvo from the program “Energy clean, safe and efficient ” of the French National Research Agency (grant ANR-17-CE05-0036). The work at Inner Mongolia Normal University was supported by the National Natural Science Foundation of China (grant n° 51961033).

References

[1] K. A. Gschneidner, V. K. Pecharsky, A. O. Tsokol, Recent developments in magnetocaloric materials, Rep. Prog. Phys. 68, 1479 (2005).

[2] A. Smith, C.R.H. Bahl, R. Bjørk, K. Engelbrecht, K. K. Nielsen, N. Pryds, Materials Challenges for High Performance Magnetocaloric Refrigeration Devices, Adv. Energy Mater. 2, 1288 (2012).

[3] V. Franco, J.S. Blázquez, J.J. Ipus, J.Y. Law, L.M. Moreno-Ramírez, A. Conde, Magnetocaloric effect: From materials research to refrigeration devices, Progress in Materials Science 93, 112 (2018).

[4] T. Gottschall, K. P. Skokov, M. Fries, A. Taubel, I. Radulov, F. Scheibel, D. Benke, S. Riegg, O. Gutfleisch, Making a Cool Choice: The Materials Library of Magnetic Refrigeration, Adv. Energy Mater. 9, 1901322 (2019).

[5] J. Lyubina, Magnetocaloric materials for energy efficient Cooling, J. Phys. D: Appl. Phys. 50, 053002 (2017).

[6] M. Küepferling, C. Bennati, F. Laviano, G. Ghigo, V. Basso, Dynamics of the magneto structural phase transition in $La(Fe_{0.9}Co_{0.015}Si_{0.085})_{13}$ observed by magneto-optical imaging, J. Appl. Phys. 115, 17A925 (2014).

[7] E. Lovell, M. Bratko, A. D. Caplin, A. Barcza, M. Katter, L. Ghivelder, L. F. Cohen, Magnetic relaxation dynamics driven by the first-order character of magnetocaloric

La(Fe,Mn,Si)$_{13}$, Philos. Trans. R. Soc. Lond. A: Math. Phys. Eng. Sci. 374, 20150307 (2016).

[8] E. Lovell, M. Bratko, A. D. Caplin, and L. F. Cohen, Nucleation and dynamics of the metamagnetic transition in magnetocaloric La(Fe,Mn,Si)$_{13}$, J. Phys. D: Appl. Phys. 50, 424004 (2017).

[9] M. G. Zavareh, Y. Skourski, K. P. Skokov, D. Yu. Karpenkov, L. Zvyagina, A. Waske, D. Haskel, M. Zhernenkov, J. Wosnitza, O. Gutfleisch, Direct Measurement of the Magnetocaloric Effect in La(Fe,Si,Co)$_{13}$ Compounds in Pulsed Magnetic Fields, Phys. Rev. Applied 8, 014037 (2017).

[10] V. Basso, M. Piazzi, C. Bennati, and C. Curcio, Hysteresis and Phase Transition Kinetics in Magnetocaloric Materials, Phys. Status Solidi (B) Basic Res. 255,1700278 (2018).

[11] M. Piazzi, C. Bennati, V. Basso, Thermodynamics of the heat-flux avalanches at the first-order magnetic transition in magnetocaloric materials, Phys. Rev. Applied 8, 044023 (2017).

[12] F. Erbesdobler, C.R.H. Bahl, R. Bjørk, and K.K. Nielsen, Detailed isofield calorimetry of La(Fe,Si,Mn)-H reveals distributed magnetocaloric phase transitions, J. Appl. Phys. 127, 095102 (2020).

[13] A. Fujita, S. Fujieda, K. Fukamichi, Influence of Supercooling on the Thermally Induced First-Order Magnetic Transition in Magnetocaloric Compound La(Fe$_{0.88}$Si$_{0.12}$)$_{13}$, IEEE Trans. Magn. 47, 3387 (2011).

[14] C. Bennati, L. Gozzelino, E. S. Olivetti, V. Basso, Heterogeneous nucleation and heat flux avalanches in La(Fe, Si)$_{13}$ magnetocaloric compounds near the critical point, Appl. Phys. Lett. 109, 231904 (2016).

[15] F. Guillou, H. Yibole, Z. Q. Ou, E. Brück, O. Tegus, Large recalescence-like event at the first cooling across the magnetic transition of (Mn,Fe)$_2$(P,Si) magnetocaloric materials, Scripta Materialia 160, 81 (2019).

[16] A. Waske, L. Giebeler, B. Weise, A. Funk, M. Hinterstein, M. Herklotz, K. Skokov, S. Fähler, O. Gutfleisch, J. Eckert, Asymmetric first-order transition and interlocked particle state in magnetocaloric La(Fe,Si)$_{13}$, Phys. Status Solidi RRL9, 136 (2015).

[17] C. Bennati, F. Laviano, G. Durin, E. Olivetti, V. Basso, G. Ghigo, and M. Küepferling, Local magnetic behavior across the first order phase transition in La(Fe$_{0.9}$Co$_{0.015}$Si$_{0.085}$)$_{13}$ magnetocaloric compound, J. Magn. Magn. Mater. 400, 339 (2016).

[18] J. Lyubina, R. Schäfer, N. Martin, L. Schultz, O. Gutfleisch, Novel Design of $La(Fe,Si)_{13}$ Alloys Towards High Magnetic Refrigeration Performance, Adv. Mater. 22, 3735 (2010).

[19] T. Gottschall, D. Benke, M. Fries, A. Taubel, I. A. Radulov, K. P. Skokov, and O. Gutfleisch, A Matter of Size and Stress: Understanding the First-Order Transition in Materials for Solid-State Refrigeration, Adv. Funct. Mater. 27, 1606735 (2017).

[20] A. Fujita, S. Fujieda, K. Fukamichi, H. Mitamura, T. Goto, Itinerant-electron metamagnetic transition and large magnetovolume effects in $La(Fe_xSi_{1-x})_{13}$ compounds, Phys. Rev. B 65, 014410 (2001).

[21] F. X. Hu, J. Gao, X. L. Qian, M. Ilyn, A. M. Tishin, J. R. Sun, B. G. Shen, Magnetocaloric effect in itinerant electron metamagnetic systems $La(Fe_{1-x}Co_x)_{11.9}Si_{1.1}$, J. Appl. Phys. 97, 10M303 (2005).

[22] H. N. Bez, K. K. Nielsen, A. Smith, P. Norby, K. Ståhl, and C. R. H. Bahl, Strain development during the phase transition of $La(Fe,Mn,Si)_{13}$-H_z , Appl. Phys. Lett. 109, 051902 (2016).

[23] W. A. Soffa and D. E. Laughlin, Diffusional Phase Transformations in the Solid State, in: D. E. Laughlin and K. Hono (Eds), Physical Metallurgy, fifth ed., 2014, pp. 851-1020.

[24] Y. Chen, C.A. Schuh, Coupled kinetic Monte Carlo-finite element mesoscale model for thermoelastic martensitic phase transformations in shape memory alloys, Acta Mater. 83, 431 (2015).

[25] E. Z. Valiev, I. F. Berger, V. I. Voronin, V. A. Glazkov, A. A. Kaloyan, K. M. Podurets, Effect of Hydrostatic Pressure on the Magnetic and Lattice Properties of the Ferromagnet $La(Fe_{0.86}Si_{0.14})_{13}$, Phys. Solid State 56, 14 (2016).

[26] B. Kaeswurm, A. Barcza, M. Vögler, P. T. Geiger, M. Katter, O. Gutfleisch, L. F. Cohen, Behaviour of the Young's modulus at the magnetocaloric transition in La $(Fe,Co,Si)_{13}$, J. Alloy Compd. 697, 427 (2017).

[27] F. Guillou, H. Yibole, N. van Dijk, L. Zhang, V. Hardy, E. Brück, About the mechanical stability of MnFe(P,Si,B) giant-magnetocaloric materials, J. Alloys Compd. 617, 569 (2014).

[28] O. Glushko, A. Funk, V. Maier-Kiener, P. Kraker, M. Krautz, J. Eckert, A. Waske, Mechanical properties of the magnetocaloric intermetallic $LaFe_{11.2}Si_{1.8}$ alloy at different length scales, Acta Materialia 165, 40 (2019).

[29] J. Lyubina, K. Nenkov, L. Schultz, O. Gutfleisch, Multiple Metamagnetic Transitions in the Magnetic Refrigerant $La(Fe,Si)_{13}H_x$, Phys. Rev. Lett. 101, 177203 (2008).

[30] J. Hao, F. Hu, J.-T. Wang, F.-R. Shen, Z. Yu, H. Zhou, H. Wu, Q. Huang, K. Qiao, J. Wang, J. He, L. He, J.-R. Sun, B. Shen, Large Enhancement of Magnetocaloric and Barocaloric Effects by Hydrostatic Pressure in $La(Fe_{0.92}Co_{0.08})_{11.9}Si_{1.1}$ with a $NaZn_{13}$-Type Structure, Chem. Mater. 32, 1807 (2020).

[31] V. Hardy, R. Hamane, X. Larose, M. Risser, F. Guillou, Burstlike first-order transformation studied by semi-adiabatic relaxation calorimetry, J. Appl. Phys. 130, 165106 (2021).

[32] J. Lai, H. Sepehri-Amin, X. Tang, J. Li, Y. Matsushita, T. Ohkubo, A. T. Saito, K. Hono, Reduction of hysteresis in $(La_{1-x}Ce_x)_y(Mn_zFe_{11.4-z})Si_{1.6}$ magnetocaloric compounds for cryogenic magnetic refrigeration, Acta Mater. 220, 117286 (2021).